JOURNAL OF MATERIALS SCIENCE 28 (1993) 5620–5629

Analysis of a mixed mode fracture specimen: the asymmetric double cantilever beam

F. XIAO, C.-Y. HUI, E. J. KRAMER*
Department of Theoretical and Applied Mechanics and the Materials Science Center, and
**Department of Materials Science and Engineering and the Materials Science Center, Cornell University, Ithaca, NY 14853, USA*

An asymmetric double cantilever beam (ADCB) is a simple but effective specimen for the measurement of polymer/polymer and polymer/non-polymer bimaterial interface fracture toughness. In order to characterize fully the bimaterial interface strength, and to control the crack trajectory, the critical energy release rate, G_c, and the phase angle, ψ, of the applied stress field as functions of loading and geometry of the specimen should be obtained. For most practical cases, ψ has to be evaluated numerically. In this work, a boundary element analysis is carried out to obtain G and ψ for the ADCB specimen at different material and geometry combinations. An expression for the energy release rate, G, based on Kanninen's beam on elastic foundation model is compared with the numerical results. Limitations on the use of the ADCB specimen are also discussed.

1. Introduction

Strong interface adhesion and a controlled morphology are important issues for phase-separated blends of immiscible homopolymers. It is well known that addition of block copolymers to these blends can cause remarkable improvement in their mechanical properties [1, 2], particularly in their fracture toughness characteristics, and, accordingly, block copolymers have been widely used as compatibilizers for these polymer blend systems. The improvement results from the fact that block copolymer chains form interface junctions through which stress can be transferred [3–6] resulting in a substantial reinforcement of the interfaces themselves.

Interface adhesion can be quantified using the concept of interface fracture toughness [7–10]. Common tests for measuring polymer/polymer adhesion have problems that are both intrinsic to the types of materials being measured and difficult to circumvent. Engineering tests such as the peel and blister test are often sensitive to the global inelastic deformations which occur in the polymer away from the crack tip. Standard fracture mechanics tests such as the single-edge notch test are often limited in their applicability, as the introduction of bimaterial interfaces often results in cohesive failure of one of the substrate materials as cracks tend to deflect into the more compliant substrate. While microscopic approaches, such as those using surface force measurement apparatus, can provide information about the molecular affinity between polymer and substrate, they may not allow the development of the local interfacial crack tip inelastic deformation mechanisms such as crazing, which have significant effects on the magnitude of the interfacial fracture toughness.

Cracks in homogeneous brittle materials grow in an opening mode and the fracture toughness, G_C, is relatively independent of the mixity of the applied loading, which can be considered as a measure of the shear and normal traction experienced near the crack tip [11, 12]. On the other hand, the fracture toughness of a bimaterial interface depends not only on the energy release rate but also on the phase angle which measures the relative amount of shear and tensile loading experienced by material points directly ahead of the interface crack [13–16]. Recently, many tests have been successfully designed to measure the interface fracture toughness of bimaterial systems. For example, Charalambides *et al.* [16] have developed a four-point bending specimen with interface cracks to investigate the interface fracture tougness of Al/poly(methylmethacrylate)(PMMA). O'Dowd *et al.* [17], have developed asymmetric and symmetric bend specimens to investigate the interface fracture toughness of the alumina/niobium system. Liechti and Chai used biaxial loading experiments to investigate the glass/epoxy interface [18]. Based on the work of Brown [19], we have found that an effective test method for the fracture toughness of a polymer/polymer interface is the asymmetric double cantilever beam specimen (ADCB) shown in Fig. 1. ADCB specimens are easy to fabricate and they cover a reasonable range of phase angles so that the trajectory of the crack can be controlled, causing it to grow along the interface. ADCB specimens have been used successfully in recent experiments to measure the interface

0022–2461

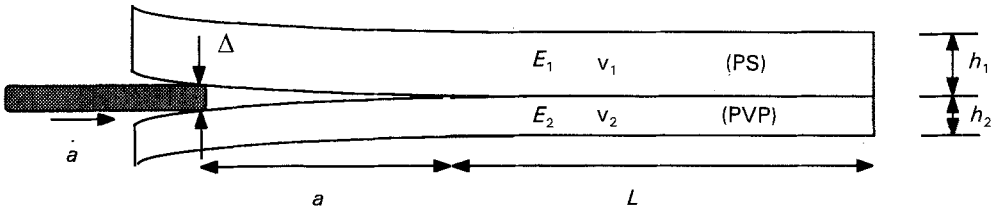

Figure 1 Schematic figure of the ADCB specimen. Δ, razor blade thickness; a, the crack length; L, the uncracked ligament length; h_1 and h_2, the thicknesses of the two beams.

fracture toughness of bimaterial systems such as polystyrene/poly(2 vinylpyridine) (PS/PVP) and PS/glass [5, 6].

The development of a test specimen for measuring interface fracture toughness involves finding analytical and numerical solutions for the energy release rate and determining the stress intensity factors and the phase angles. In this work we focus on the determination of these loading parameters, using the PS/PVP as an illustrative case. The experimental results and details using the ADCB specimen such as specimen preparation, testing procedure, and data analysis (ion beam analysis, transmission electron microscopy, etc.) can be found elsewhere [5, 6, 20–23].

2. Mechanics – mixed mode fracture

The near-tip stress field of a stationary crack lying along a planar bimaterial interface between two linearly elastic, isotropic and homogeneous materials can be uniquely characterized by the complex stress intensity factor [7]

$$K = K_1 + iK_2 \tag{1}$$

where $i = (-1)^{1/2}$; K is a function of the specimen geometry, the applied load and material properties. K_1 and K_2 have the dimension of [stress] [length]$^{1/2-i\varepsilon}$ where ε is a real number related to the material properties by

$$\varepsilon = (1/2\pi)\, ln[(\kappa_1/\mu_1 + 1/\mu_2)/(\kappa_2/\mu_2 + 1/\mu_1)] \tag{2}$$

where $\kappa_i = 3 - 4\nu_i$ for plane strain and $\kappa_i = (3 - \nu_i)/(1 + \nu_i)$ for plane stress. ν_i and μ_i denote Poisson's ratio and the shear modulus of Materials 1 and 2, respectively. The parameter ε is very small for most bimaterial systems. For example, for PS/PVP system, with PS in the upper beam and PVP in the lower beam as shown in Fig. 1, the Young's modulus for PS is $E_1 = E_{PS} = 3$ GPa, and Poisson's ratio $\nu_1 = \nu_{PS} = 0.341$; for PVP, $E_2 = E_{PVP} = 3.5$ GPa, and $\nu_2 = \nu_{PVP} = 0.325$, $\varepsilon = 2.8 \times 10^{-3}$ for the system.

The traction directly ahead of the crack tip is given by

$$(\sigma_{yy} + i\sigma_{xy})_{\theta=0} = Kr^{-1/2+i\varepsilon} \tag{3}$$

where r and θ are a polar coordinate system with origin at the crack tip as shown in Fig. 2. The crack opening displacement components at a small distance r behind the crack tip are given by

$$\begin{aligned}\Delta v + i\Delta u &= \Delta u_y + i\Delta u_x \\ &= (u_y + iu_x)_{\theta=\pi} - (u_y + iu_x)_{\theta=-\pi} \\ &= C\,Kr^{1/2+i\varepsilon}[2\,(2\pi)^{1/2}\,(1 + 2i\varepsilon)\cosh(\pi\varepsilon)]\end{aligned} \tag{4}$$

where C is a material constant defined by $C = (\kappa_1 + 1)/\mu_1 + (\kappa_2 + 1)/\mu_2$. Δv and Δu at $r = D$ are shown schematically in Fig. 2.

Equation 3 implies that the near-tip stress oscillates very rapidly due to the term $r^{i\varepsilon} = \cos[\varepsilon ln(r)] + i\sin[\varepsilon ln(r)]$ as one approaches the crack tip $r = 0$. For the same reason, Equation 4 shows that there is a region near the crack tip where material interpenetration occurs. However, for most material systems and loading combinations encountered in the polymer ADCB specimen testing, this near-tip contact zone is smaller than any meaningful physical scale and can be ignored [7]. The ratio of the shear traction to the normal traction directly ahead of the crack tip at $x = d$ is given by

$$\begin{aligned}(\sigma_{xy}/\sigma_{yy})_{r=d,\,\theta=0} &= \tan\psi \\ &= \mathrm{Im}[Kd^{i\varepsilon}]/\mathrm{Re}[Kd^{i\varepsilon}]\end{aligned} \tag{5}$$

where Re and Im denote the real and imaginary part of a complex number and ψ is defined as the phase angle of $Kd^{i\varepsilon}$. It is important to note that unless $\varepsilon = 0$, the phase angle, ψ, depends on d and hence a unique value of phase angle (usually referred to as mixity if such a unique value exists) cannot be defined. If $\varepsilon = 0$, K_1 and K_2 become the classical stress intensity factors K_I, K_{II} which strictly measure the normal and shear stress singularity. A particular case where $\varepsilon = 0$ is when the material is homogeneous.

In a homogeneous material, $\psi > 0$ implies that the crack has a tendency to propagate into the material below the interface, follow the direction perpendicular to that of the maximum "hoop" stress; whereas if $\psi < 0$, the crack has a tendency to be deflected into the material above the interface [11]. For bimaterial systems, the phase angle, ψ, varies slowly along the interface. In general, the direction of crack deflection depends on the phase angle as well as the details of the failure and deformation mechanisms of the interface and those of the bulk materials above and below the interface. However, ψ can often be used as a guide to predict roughly the crack propagation direction. In experiments, it is often convenient to measure the energy release rate, G, which is related to the complex stress intensity factor, K, by

$$G = C\,|K|^2/[16\cosh^2(\pi\varepsilon)] \tag{6a}$$

or

$$|K| = (G/C)^{1/2}\,4\cosh(\pi\varepsilon) \tag{6b}$$

where $|\ |$ denote the absolute value of a complex number. Because G is a real number, it alone cannot characterize fully the crack-tip field. In order to specify K, which has two real components, the phase angle, ψ,

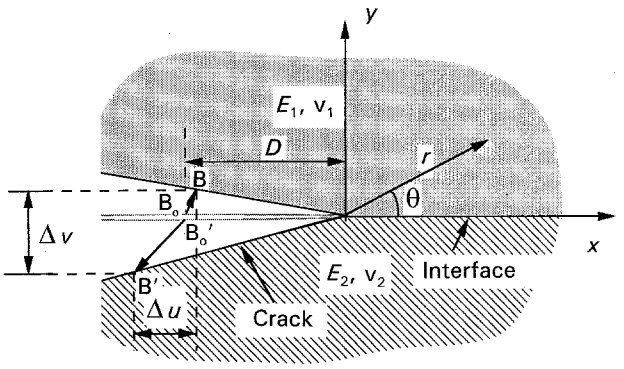

Figure 2 Schematic figure showing the coordinate system at the crack tip. B_0 and B_2' denote points on opposite sides of crack face before loading. B and B' denote points on opposite sides of crack face after loading. Δv, the opening displacement; Δu, the shearing displacement at a distance D behind the crack tip.

corresponding to a fixed d is needed. Using this definition, a point in the (G, ψ) plane is uniquely related to a point in the (K_1, K_2) plane. It should be noted that the choice of d is arbitrary [10]. From physical considerations, it is often chosen to be comparable with the size of the plastic zone ahead of the crack which is typically the smallest macroscopic length scale in the physical problem. To compare experimental interface fracture toughness results, one should use the phase angle, ψ, corresponding to the same d for a given material combination. The phase angles, ψ, corresponding to two different choices of d, i.e. d_1 and d_2 are related by

$$\psi(d_1) - \psi(d_2) = \varepsilon \ln[d_1/d_2] \tag{7}$$

Because typically ε is very small (as in the PS/PVP system), and ln is a "weak" function of its argument, the phase angle usually does not change significantly if different values of d are used [7].

Following the concept of "failure locus" introduced by Rice [7], for a given phase angle, ψ (associated with the chosen d), the applied G reaches a critical value, $G_c(\psi)$, which is a material constant and is defined as interface fracture toughness. Because G_c depends on ψ, the fracture toughness is a curve in the (G, ψ) plane.

3. ADCB specimen description

The ADCB specimen is shown schematically in Fig. 1. Two slabs of different thicknesses are bonded to form an ADCB. One example of the application of the test is conducted with the PS/PVP polymer pair. A razor blade of known thickness, Δ, is driven at a very slow constant rate forcing an interface crack to grow, the length of which may be measured by means of a video camera and monitor. One advantage of this test is that at least 20 values of fracture toughness could be obtained from each specimen to calculate the mean value of G, and hence increase the accuracy of the test.

The thicknesses of the two beams are h_1 and h_2, the distance from the loading point to the crack tip is a, the length of the uncracked ligament of the specimen is L. The thickness of the inserted razor blade is Δ. E_1, E_2 and ν_1, ν_2 are the Young's moduli and Poisson's ratios of the upper and lower beam.

Note that from dimensional analysis, the solution of the bimaterial problem depends on the dimensionless parameters E_1/E_2, ν_1, ν_2, h_2/h_1, h_1/a and L/a. For example, from linearity and dimension considerations, the complex K for the ADCB specimen has the form

$$K = E_1 \delta a^{-2} h_1^{3/2 - i\varepsilon} F(E_1/E_2, \nu_1, \nu_2, h_2/h_1, h_1/a, L/a) \tag{8}$$

where $\delta = \delta v + i\delta u$ is the prescribed displacement vector at the loading point. In our ADCB case $\delta = \Delta$, the razor blade thickness. The complex function, F, is a dimensionless function of its dimensionless arguments. F can be obtained using Equations 5 and 6b once G and the phase angle, ψ, are determined numerically.

3.1. Approximate expressions for G

The energy release rate, G, can be estimated by treating the ADCB as two separate elastic cantilever beams and finding the derivative of the strain energy stored in the beams with respect to the crack length, a. The resulting expression for G is

$$G = \frac{3\Delta^2 E_1 E_2 h_1^3 h_2^3}{8a^4(E_1 h_1^3 + E_2 h_2^3)} \tag{9}$$

Equation 9 is a good approximation for cracks with lengths much longer than the beam thickness. Because most polymer glasses have low elastic moduli compared with metals, the crack length, a, needed for crack growth along sufficiently strong interfaces for a given thickness of the razor blade may not be large enough for the simple beam theory to be accurate. In other words, the simple beam model is too stiff to capture the actual energy release rate, G, for short cracks. A possibly more accurate estimate was given by Creton *et al.* [5], which was obtained based on Kanninen's beam on elastic foundation model [24].

$$G = \frac{3\Delta^2 E_1 E_2 h_1^3 h_2^3 (C_1^2 E_2 h_2^3 + C_2^2 E_1 h_1^3)}{8a^4 \Lambda^2} \tag{10}$$

where $\Lambda = C_1^3 E_2 h_2^3 + C_2^3 E_1 h_1^3$ and $C_1 = 1 + 0.64 h_1/a$, $C_2 = 1 + 0.64 h_2/a$. Indeed, experimental fracture toughness data obtained by Creton [5] have been found to correlate considerably better when Equation 10 is used for the determination of energy release rate.

It should be noted that Equations 9 and 10 both implicitly assume that the length of the uncracked ligament of the beam, L, is large compared with the crack length, a, and $h_i/a < 1$, so that crack growth proceeds in an approximate steady state manner. This assumption allows us to calculate the mean fracture toughness from the 20 or so data points obtained from the test.

4. Numerical results for G and ψ

A boundary element method is developed to calculate G and ψ for the ADCB specimens for different values of h_1/h_2, E_1/E_2, ν_1, ν_2 and h_1/a. Details of this method are given in the Appendix. We did not include

L/a in this parameter study because our numerical results showed that G and ψ do not change significantly as long as $L/a \geq 1$, a condition that is satisfied by most ADCB specimens. Also, to limit the number of parameters in this numerical study, we assumed that $\nu_1 = \nu_2 = 0.3$, which is close to Poisson's ratio for most materials.

In the following, the approximate expression for the energy release rate from Equation 10, G_K and the energy release rate obtained from the BEM result, G_{BEM} will be normalized by G_{beam}, which is the energy release rate from the simple beam theory given by Equation 9; these normalized energy release rates are denoted by G_K^* and G_{BEM}^*, respectively.

We first compared the validity of the approximate formula for the energy release rate given by Equations 9 and 10 with the BEM results. These results are shown in Fig. 3a–c. Because G_{beam} is the normalization factor, the top horizontal lines $G^* = 1$ in these figures are the normalized energy release rate predicted by simple beam theory. Two thickness combinations are used in these figures, namely, $h_2 = h_1$ and $h_2 = 10h_1$. The solid line represents G_K^* for $h_2 = h_1$, and the dashed line represents the G_K^* for $h_2 = 10h_1$.

Fig. 3a shows G^* for $E_1 = E_2$. The G_{BEM}^* and G_K^* are in close agreement in the short-crack range, i.e. from $2 \leq a/h_1 \leq 6$. This figure clearly shows that the energy release rate given by simple beam theory overestimates the energy release rate, particularly in the short-crack range. As the crack length increases, G_{BEM}^* and G_K^* approach G_{beam}^* which is 1, with G_{BEM}^* lying intermediate between G_K^* and G_{beam}^*. Thus, G_K is a good approximation for G_{BEM} over nearly all the practical range of a/h_1 and h_1/h_2. It should be noted that the difference between G_{BEM}^* and G_K^* is approximately independent of the ratio of the beam thicknesses.

Although the differences between the normalized energy release rate, G_{BEM}^* and G_K^*, are larger for long cracks than those for the short cracks, as can be seen from Fig. 3a, the differences between energy release rate G_{BEM} and G_K for long cracks are actually very small because the normalization factor, G_{beam}, is small for large crack length. For example, in the specimens we used for the PS/PVP system, the energy release rate $G_K \approx 1.2\,J\,m^{-2}$ and $G_{BEM} \approx 1.1\,J\,m^{-2}$ for $a/h_1 = 6$ (where $h_1 = 1.6$ mm). Therefore, the absolute value of the differences between G_{BEM} and G_K for long cracks are negligible.

Fig. 3b shows G^* for $E_1 = 5E_2$. As in the case of $E_1 = E_2$, G_K and G_{BEM} are in close agreement if $h_2 = h_1$. However, for large ratio of beam thicknesses, e.g. $h_2 = 10h_1$, G_K and G_{BEM} differ significantly from each other for short cracks. Even in these cases, G_K^* is still a much better approximation to G_{BEM}^* than G_{beam}^*, which is 1. As before, this curve shows that the simple beam theory is not a good approximation for short cracks, especially when the differences of beam thicknesses and the elastic moduli are large.

Fig. 3c shows the results for G^* for $E_1 = 25\,E_2$. G_K^* and G_{BEM}^* are in reasonable agreement for different values of a/h_1 only if h_1/h_2 is close to unity. For a short crack along a symmetric double cantilever beam interface, e.g. $a = 2h_1$, $h_2 = h_1$, $G_{beam} \approx 2.5\,G_{BEM}$; for ADCB ($h_2 = 10h_1$) short crack ($a = 2h_1$), $G_{beam} \approx 20\,G_{BEM}$.

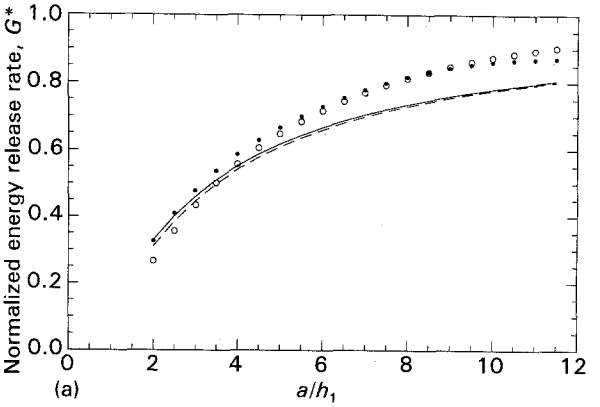

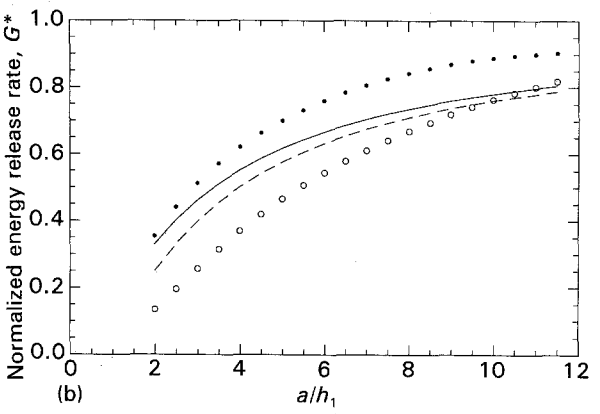

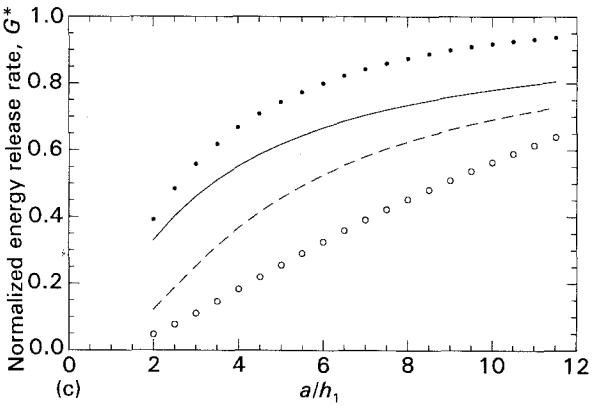

Figure 3 Comparison of G_{beam}^*, G_{BEM}^*, and G_K^*, for three different material pairs. $G_{beam}^* = 1$. G_K^*: (——) for $h_2 = h_1$, (– – –) for $h_2 = 10h_1$. G_{BEM}^*: (●) for $h_2 = h_1$, (○) for $h_2 = 10h_1$. (a) $E_1 = E_2$, (b) $E_1 = 5E_2$, and (c) $E_1 = 25E_2$.

From Fig. 3 one can see that for short cracks, i.e. $a/h_1 < 6$, there are substantial differences between G_{beam} and G_{BEM}; however, G_K and G_{BEM} in this range are still in good agreement as long as there is no substantial difference in elastic moduli across the interface. Even if $E_1/E_2 \gg 1$, Kanninen's approximation Equation 10 is still reasonably accurate as long as $0.5 \leq h_2/h_1 \leq 2$. This result implies that G_K can be used to determine interface fracture toughness for most bimaterial systems composed of polymer glasses.

The BEM numerical results of normalized energy release rate, G^* and phase angle, ψ_d, of the ADCB

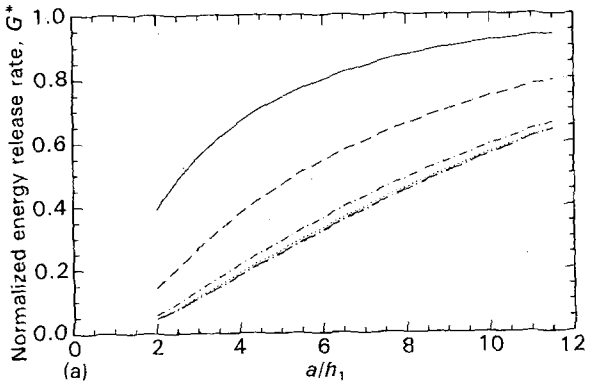

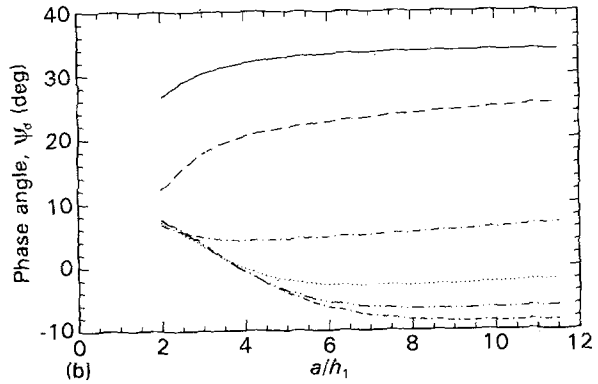

Figure 4(a,b) $E_1 = 25E_2$.

Figures 4–12 Numerical results of energy release rate, G^*, and phase angle, ψ_d, for different geometry combinations. The thickness combinations are $h_2/h_1 = 1, 2, 4, 6, 8, 10$. G^*_{BEM}, and ψ_d: (——) for $h_2 = h_1$; (– – –) for $h_2 = 2h_1$; (–·–) for $h_2 = 4h_1$; (· · ·) for $h_2 = 6h_1$; (–···–) for $h_2 = 8h_1$, (–··––) for $h_2 = 10h_1$. The material combinations used in Figs 4–12 are given below each figure.

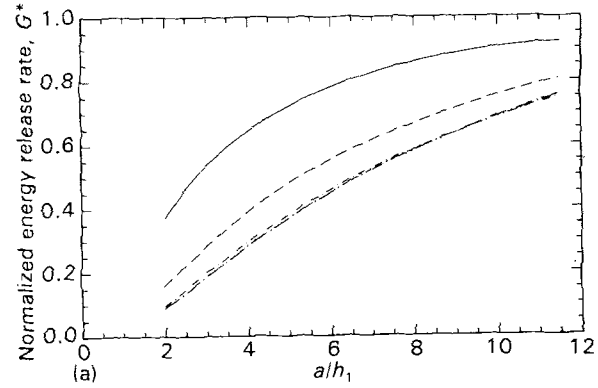

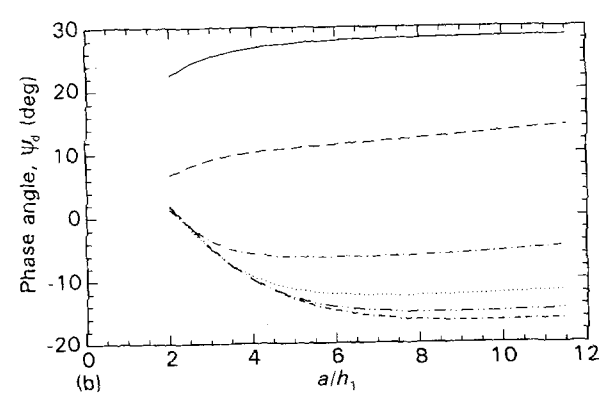

Figure 5(a,b) $E_1 = 10E_2$.

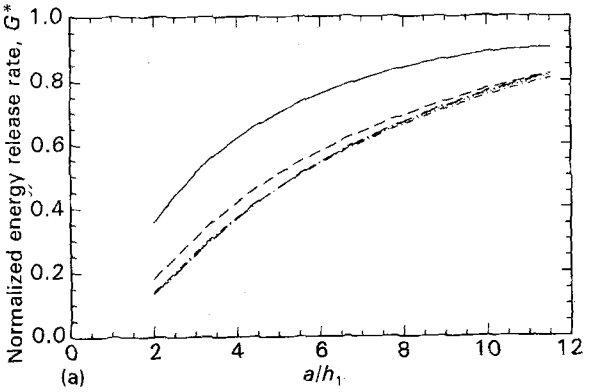

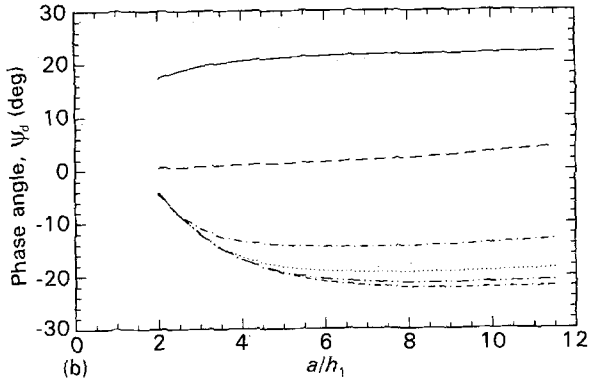

Figure 6(a,b) $E_1 = 5E_2$.

specimen for nine different material combinations, i.e. $E_1/E_2 = 25$, 10, 5, 2, 1, 0.5, 0.2, 0.1 and 0.04, are computed and given in Figs 4–12. Each figure contains the results for one material pair at six thickness combinations $h_2/h_1 = 1, 2, 4, 6, 8, 10$. The numerical results of G^* and ψ_d are given in the sub-figures (a) and (b), respectively. The horizontal axis is the normalized crack length, a/h_1, while the vertical axis is the normalized energy release rate, G^* (Figs 4a–12a) or the phase angle, ψ_d (Figs 4b–12b).

The phase angle, $\psi_d = \tan^{-1}[\mathrm{Im}\,K^*/\mathrm{Re}\,K^*]$, is determined at $x = d$, where $K^* = K\,d^{i\varepsilon}$ and d is of the order of the plastic zone size and is chosen to be 100 μm in this work. This value of d is of the order of the largest craze zone size observed in experiments. This choice will be justified in the discussion.

The G^*_{BEM} and ψ_d results for the six thickness combinations ($h_2/h_1 = 1, 2, 4, 6, 8, 10$) are represented by the six different lines in both G^* and ψ_d figures in Figs 4a, b–12a, b.

Numerical results for $E_1 = 25E_2$ are shown in Fig. 4 for the case of severe material mismatch where the upper beam is practically rigid compared with the lower beam. Obviously, the simple beam model should not be used. As the crack length increases, the BEM result approaches that given by the simple beam model for geometrically symmetric samples ($h_2 = h_1$), while G_{BEM} is still much less than G_{beam} for geometrically highly asymmetric specimens. For these specimens, the G^* curves collapse into one, i.e. the normalized energy release rate, G^*, is approximately independent of h_2/h_1 ratio for $h_2 \geq 6h_1$.

The phase angles, ψ_d, for the case of $E_1 = 25E_2$ are given in Fig. 4b. For $h_2 \leq 4h_1$, $\psi_d > 0$, which means

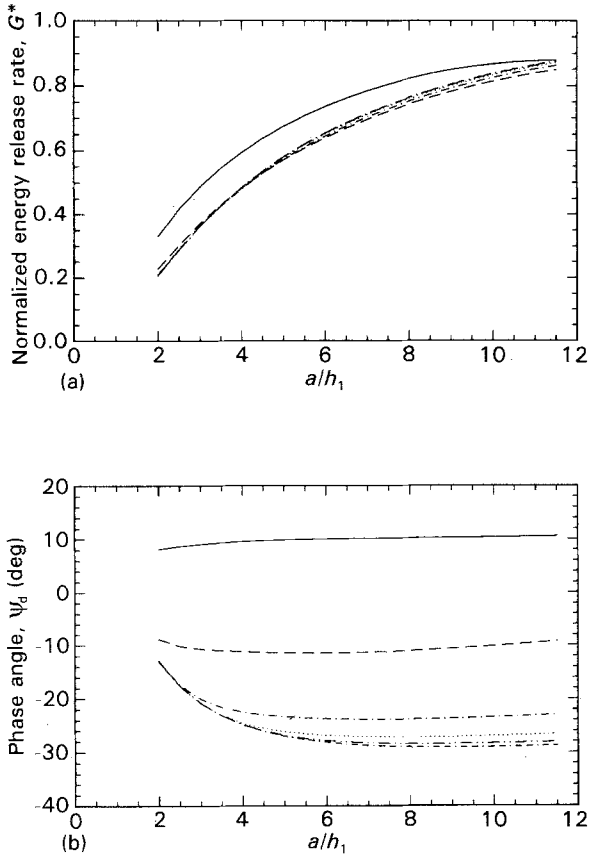

Figure 7(a,b) $E_1 = 2E_2$.

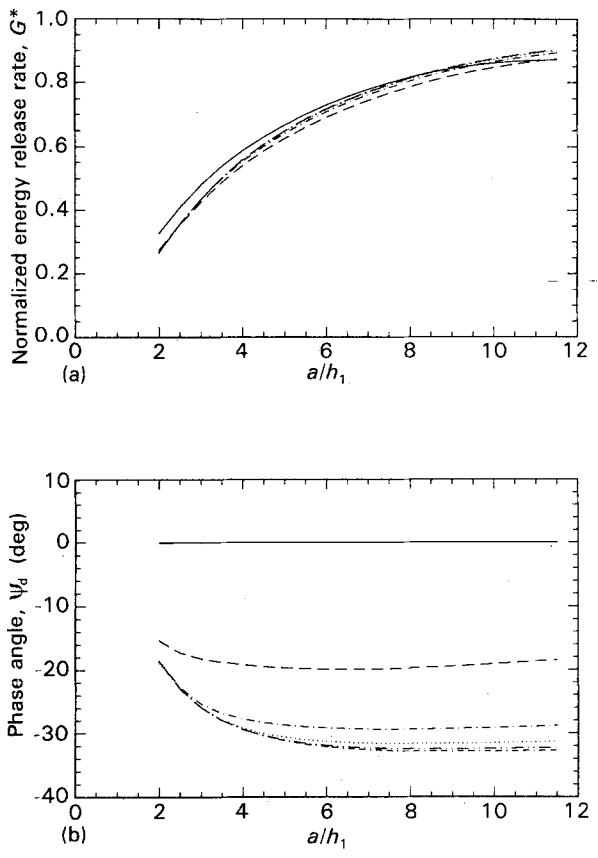

Figure 8(a,b) $E_1 = E_2$.

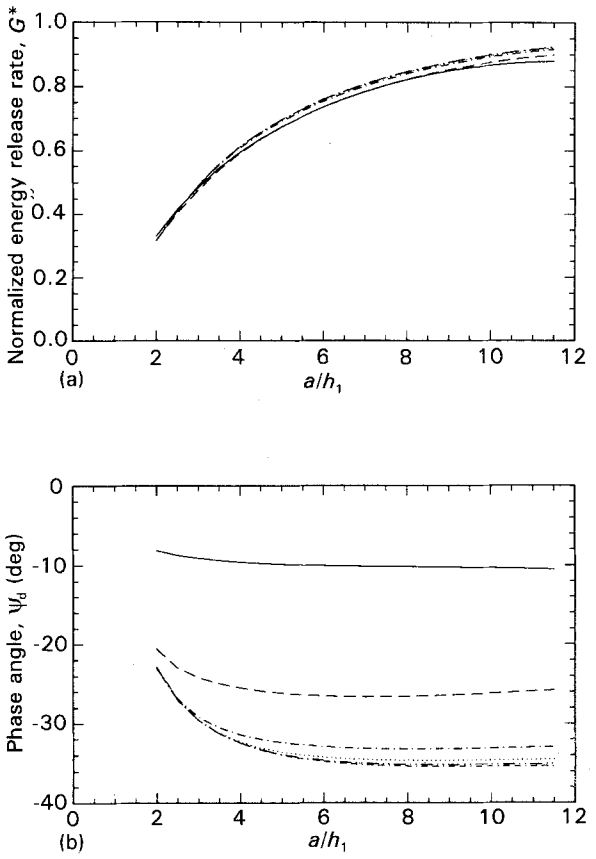

Figure 9(a,b) $E_1 = E_2/2$.

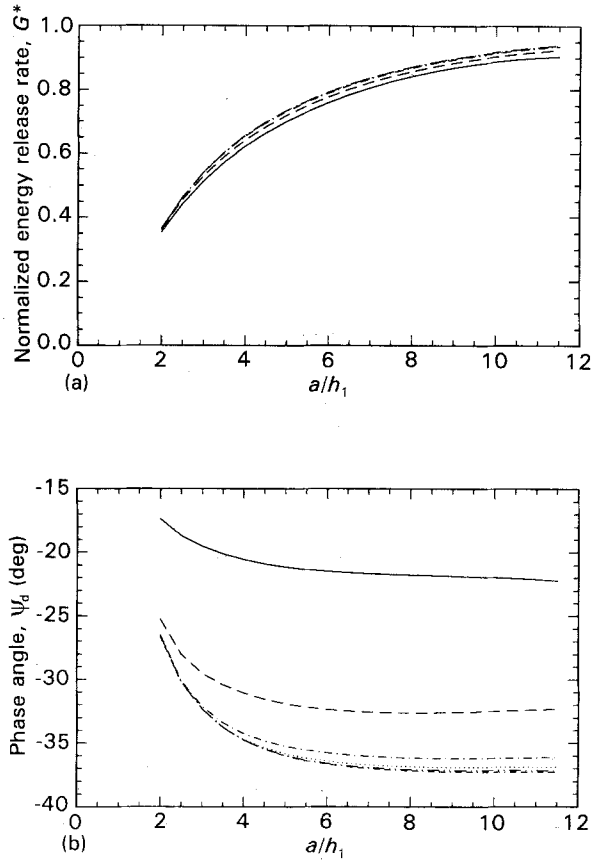

Figure 10(a,b) $E_1 = E_2/5$.

the stress state at $r = d$, $\theta = 0$ has a tendency to drive the crack into the lower beam (the lower modulus material). ψ_d decreases as the aspect ratio h_2/h_1 and the crack length increase and is negative for $h_2 \geq 6h_1$ and $a \geq 4h_1$. For long cracks ($a \geq 6h_1$), the phase angle does not change significantly for each geometry. The maximum phase angle is about 35° and the minimum is about $-8°$.

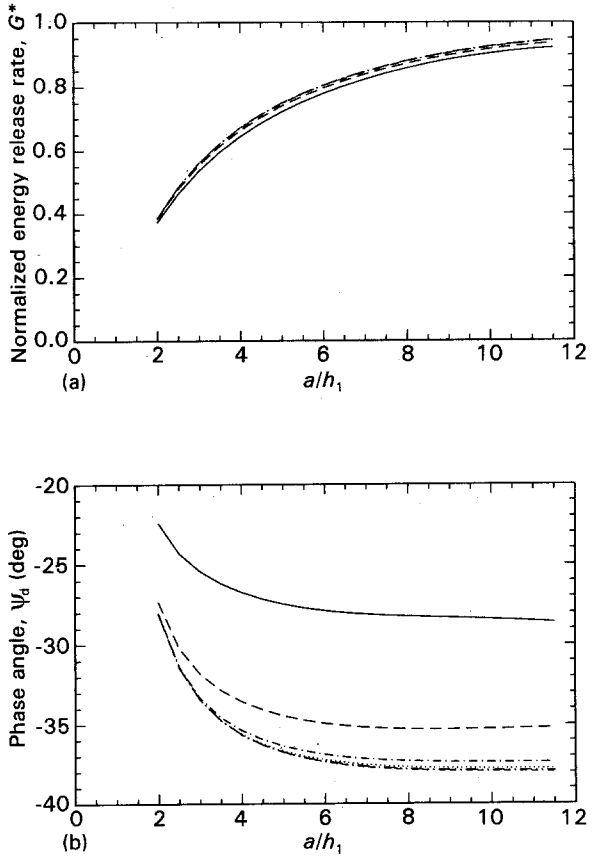

Figure 11(a,b) $E_1 = E_2/10$.

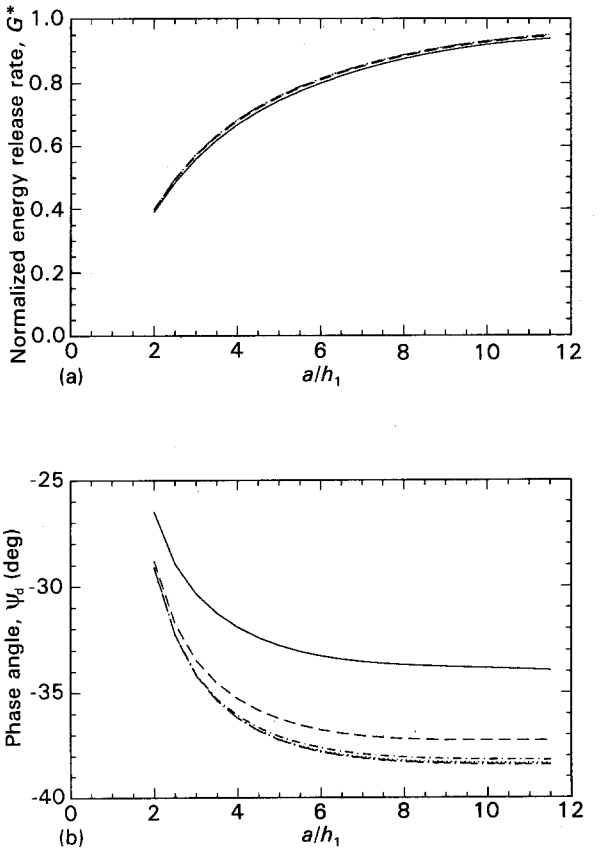

Figure 12(a,b) $E_1 = E_2/25$.

Fig. 5 gives the numerical results for $E_1 = 10E_2$. The general trend for the energy release rate diagram is similar to that of the $E_1 = 25E_2$ case. The G^* curves collapse into one when $h_2 \geq 4h_1$. The phase angle, ψ_d, is only positive when $h_2 \leq 2h_1$. The phase angle is negative for higher aspect ratios. Similar trends are observed in Fig. 6 for $E_1 = 5E_2$.

In Fig. 7, $E_1 = 2E_2$, the normalized energy release rate curves for $h_2 \geq 2h_1$ overlap each other and the $G_{\text{beam}}/G_{\text{BEM}}$ ratio reduces to 5 for short severe asymmetric specimen. For long cracks, i.e. $a \geq 5h_1$, the phase angles remain constants for different thickness ratios.

Fig. 8 provides the G and ψ_d curves for the special case of $E_1 = E_2$. The six G^* curves are practically independent of the thickness ratio. The phase angle ψ_d is independent of the choice of d and it represents the real shear/tensile mode mixity in this case. The phase angle, ψ_d, is also close to constant if $a/h_1 \geq 4$, the case of a relatively long crack.

In Figs 9–12, $E_2 > E_1$, the material in the lower beam is stiffer than that of the upper beam. For these cases, the normalized energy release rate, G^*, is practically independent of the beam thickness ratio that we have selected, i.e. $h_2 > h_1$. Furthermore, for these thickness ratios, the energy release rate G_{BEM} is better approximated by G_{beam} for the case of long cracks than for the cases where $E_2 < E_1$. For short cracks, however, there is still a substantial difference between G_{BEM} and G_{beam}.

Figs 9b–12b provide phase angle information for material pairs with $E_2/E_1 = 2, 5, 10$ and 25. The lower beam is stiffer and its thickness is equal to or bigger than that of the upper beam, so the phase angles are always negative for these specimens. From Figs 9b–12b, the region of a/h_1, where the phase angle remains constant, decreases with increasing material property mismatch and aspect ratio. For samples with $h_2 \geq 6h_1$, there is no significant change in phase angle with further increases in geometric asymmetry. The most negative angle, ψ_d, we obtained in the calculation is about $-38°$ with $E_2 = 25E_1$, $h_2 \geq 6h_1$ and $h \ll a$. The range of phase angle possible for the ADCB specimens is thus estimated to be $(-38°, 35°)$.

5. Discussion

5.1. Characteristic length, d

To be consistent with the small-scale yielding assumption, the distance, d, used to compute the phase angle is chosen to be larger than the length of a typical craze zone ahead of the interface crack but smaller than the typical specimen dimensions. (Our specimen dimensions are in the millimetre range.)

The d value should be larger than the craze zone length, so the material there is in linear elastic state. For the bimaterial PS/PVP system, the material property mismatch is small, so that the craze zone length, L_c, ahead of the interface crack can be estimated using the Dugdale model of a crack lying in a homogeneous material loaded under mode I conditions [25, 26]

$$L_c \approx \pi E G/[8(1-\nu^2)\sigma_0^2] \qquad (11)$$

where G is the energy release rate, E and ν are the Young's modulus and Poisson's ratio of PS, and σ_0 is the crazing stress of PS. The crazing stress for PS

(about 55 MPa) is lower than that for PVP (about 75 MPa) under our testing conditions [5]. Using $E_{PS} = 3$ GPa and $G = 100\,J\,m^{-2}$, which is approximately the highest fracture toughness encountered for the PS/PVP system, the estimated craze zone length given by Equation 11 is about 40 μm. The choice of $d = 100$ μm is based on these considerations.

5.2. Limitation of the ADCB specimen

A related issue is the maximum toughness value that can be measured by the ADCB specimen. The maximum toughness is limited by beam failure occurring behind the crack tip caused by existing flaws or massive crazing on the beam surface. The normal stress, σ_{xx}, due to the K field on the crack surface at distance > 10 μm behind the crack tip is found to be very small compared to the stress given by the beam theory if the absolute value of the phase angle is less than 30°. Therefore, an upper bound for σ_{xx} behind the crack tip can be estimated using beam theory. Based on Kanninen's model which we used to obtain Equation 10, σ_{xx} is estimated to be

for the upper beam

$$\sigma_{max1} = \left[\frac{6E_1E_2(G/h_1)}{C_1^2E_2 + C_2^2E_1\eta^3}\right]^{1/2} \quad (12)$$

for the lower beam

$$\sigma_{max2} = \left[\frac{6E_1E_2(G/h_2)}{C_1^2E_2/\eta^3 + C_2^2E_1}\right]^{1/2} \quad (13)$$

where $\eta = h_1/h_2$ and the subscripts 1 and 2 denote the upper and lower beam. The maximum stress, $\sigma_{max\,i}$ ($i = 1$ or 2), cannot exceed the crazing stress or the stress needed to propogate an existing surface flaw. If σ_{c1} and σ_{c2} are the smaller values of the crazing stress or the stress required to propagate a pre-existing flaw in the upper and the lower material, respectively, then the conditions $\sigma_{max1} < \sigma_{c1}$ and $\sigma_{max2} < \sigma_{c2}$ must be satisfied in the upper and lower beam to prevent the substrate failure. From Equation 12, the maximum toughness, G, limited by the upper beam "strength" is,

$$G_{max1} = \sigma_{c1}^2 h_1(C_1^2E_2 + C_2^2E_1\eta^3)/(6E_1E_2) \quad (14)$$

and from Equation 13, the maximum G limited by the lower beam "strength" is

$$G_{max2} = \sigma_{c2}^2 h_2(C_1^2E_2/\eta^3 + C_2^2E_1)/(6E_1E_2) \quad (15)$$

The maximum G_c that can be measured using the ADCB cannot exceed the smaller one of G_{max1} and G_{max2}, otherwise beam fracture may occur. These equations show that one way of increasing the range of fracture toughness, G, that can be measured is to increase the beam thickness. For brittle materials, the maximum measurable G_c can be increased by increasing σ_c through surface treatment to reduce flaw size. Indeed Smith *et al.* [6] found in their experiment with PS/glass samples that higher interface fracture toughness can be measured by polishing the surface of the glass beam.

5.3. Application of ADCB specimen in experiment

The procedure for using an ADCB specimen is as follows.

1. Measure the geometric quantities, i.e. the crack length, a, beam thicknesses, h_1 and h_2, and the opening displacement, Δ, at the loading point (razor blade thickness). From these quantities as well as the material properties (E_1, E_2, ν_1, ν_2), calculate the critical energy release rate, G_c, either by numerical methods (boundary element method or finite element method) or estimate it using Equation 10.
2. Compute the phase angle, ψ, corresponding to each G_c is step 1 by numerical methods or estimate it using the data given in Figs 4–12 in this paper.
3. Plot ψ versus G_c. This diagram represents the interface fracture toughness of the bimaterial system. (Clearly, the interface fracture toughness is also a function of the interface bonding condition.)

6. Conclusions

We have computed G and ψ_d for the ADCB specimens. For short cracks and a mismatch of elastic properties that are not too severe, it is found that Equation 10, which is based on Kanninen's model, provides an accurate estimate of the energy release rate, G. Our numerical results show that this estimate is more accurate than the estimate based on the simple beam model, particularly for the cases of short cracks. The phase angle, ψ_d, for different specimen geometries and material properties is given graphically. The phase angle is found to lie between $-38°$ and $35°$ for $d = 100$ μm. For most polymer glass bimaterial systems, where moduli differences are small, approximate steady state condition of the phase angle (constant) in the experiment with ADCB specimen is guaranteed for $a/h_1 > 4$. There is a maximum value of the interface toughness that can be measured using the ADCB (corresponding to fracture of one of the beams). But the maximum value may be increased by increasing the thickness dimension of both beams and keeping the thickness ratio constant without changing the phase angle, ψ, significantly.

Acknowledgements

We gratefully acknowledge the support of the Cornell Materials Science Center (MSC) which is funded by the National Science Foundation (DMR-MRL program). We also benefitted from the use of MSC Central Facilities. E. J. Kramer acknowledges the support of the Army Research Office under grant DAAL03-91-G-0095. The authors appreciate stimulating discussions with J. Smith, C. Creton and J. Washiyama.

Appendix

The boundary element method is the numerical technique employed in this work. The advantage of this method is that it only discretizes the boundary of the elastic body. So if one is only interested in the displacements and tractions along the boundary (the

interface and crack faces in our case), the BEM is a convenient and economical method.

The bimaterial elastic body is divided into two domains, each of them is isotropic homogeneous. The integral equations are given separately in the two elastic domains as illustrated schematically in Fig. A1. The continuity of the interfacial displacements and tractions are used to couple the two sets of equations. The elements in the program are quadratic isoparametric elements. For the four elements at the crack tip, namely the elements composed of nodes a, b, c; a', b', c'; a, d, e; a', d', e', the middle nodes b, b', d, d' were placed at one-quarter the length of the elements from the crack tip as illustrated in Fig. A1, to capture the $r^{1/2}$ behaviour of the crack-opening displacement.

The boundary condition for the problem is shown in Fig. A2. The displacement at the point A is 0 in both the vertical and horizontal directions. The vertical displacement between points B and C equals the razor blade thickness, Δ.

The first method we used to compute G and ψ_d is the displacement method. From the elastic solution of the bimaterial interface crack problem, the crack opening displacement at distance, r, behind the crack tip is

$$\Delta u_y + i\Delta u_x = |(\Delta u_y)^2 + (\Delta u_x)^2|^{1/2} \exp(i\phi) \quad \text{(A1)}$$

$$\phi = \text{Arctan}(\Delta u_x/\Delta u_y) \quad \text{(A2)}$$

Using Equations A1, 4 and 5, the relation between ψ_d and ϕ is

$$\psi_d = \phi - \varepsilon \ln(r/d) + \text{Arctan}(2\varepsilon) \quad \text{(A3)}$$

where $d = 100\ \mu m$ in our calculation.

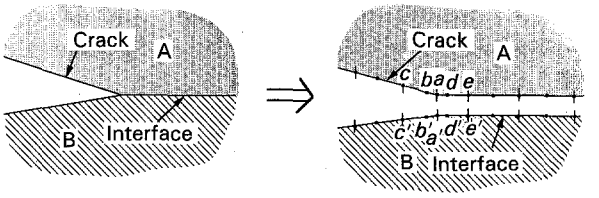

Figure A1 Configuration for BEM implementation in the crack-tip region. (a) The bimaterial crack-tip region. (b) The elastic body is divided into two subregions. The quadratic element boundaries are marked by the small vertical lines and the nodes are denoted by the small black dots. Nodes a and a' are at the crack tip. a, b, c are the nodes in the crack face in Material A. a, d, e are the nodes along the interface in Material A. $ab = ac/4$, and $ad = ae/4$. a', b', c' and a', d', c' are the corresponding nodes in Material B. The displacements in the interface nodes a and a', d and d', e and e', etc., are the same and the tractions at corresponding nodes have the same magnitude and opposite sign, respectively.

From Equation 4, one can easily express $|K|$ in terms of Δu_x and Δu_y

$$|K| = 2(2\pi)^{1/2} \cosh(\pi\varepsilon)\{(1 + 4\varepsilon^2) [(\Delta u_y)^2 + (\Delta u_x)^2]/(rC)\}^{1/2} \quad \text{(A4)}$$

Using Equations 6a and A4, G can be evaluated from Δu_x and Δu_y

$$G = \pi/2\ \{(1 + 4\varepsilon^2)[(\Delta u_y)^2 (\Delta u_x)^2]/(r)\} \quad \text{(A5)}$$

Using Equation A5, several G values are calculated from the values of Δu_x and Δu_y at different nodal points.

A second method, the virtual crack closure method, was also used to calculate G from the nodal stresses and displacements near the crack tip [27]. In this method

$$G = \boldsymbol{a}^T \boldsymbol{A}\, \boldsymbol{b} \quad \text{(A6)}$$

The vectors $\boldsymbol{a}$ and $\boldsymbol{b}$ are defined by $\boldsymbol{a} = \boldsymbol{C}\,\Delta\boldsymbol{u}$, $\boldsymbol{b} = \boldsymbol{C}\sigma$, where $\boldsymbol{A}$ and $\boldsymbol{C}$ are 6×6 matrices given below and the superscript T denotes the transpose of a vector.

The opening displacements between nodes a and a', b and b', c and c' in Fig. A1 are denoted by vector $\Delta\boldsymbol{u}$, which has six components

$$\Delta\boldsymbol{u}^T = \{\Delta\boldsymbol{u}_a, \Delta\boldsymbol{u}_b, \Delta\boldsymbol{u}_c\},$$

where $\Delta\boldsymbol{u}_a = \{\Delta u_{ax}, \Delta u_{ay},\}$, Δu_{ax} is the opening displacement in the x direction and Δu_{ay} is the opening displacement in the y direction between nodes a and a'. The stresses at nodes a, d, e as in Fig. A1 are denoted by vector $\boldsymbol{\sigma}^T = \{\boldsymbol{\sigma}_a, \boldsymbol{\sigma}_d, \boldsymbol{\sigma}_e\}$ where $\boldsymbol{\sigma}_a = \{\sigma_{ax}, \sigma_{ay}\}$, σ_{ax} and σ_{ay} are the shear and normal stress σ_{xy} and σ_{yy} at node a.

The matrices $\boldsymbol{A}$ and $\boldsymbol{C}$ are defined as

$$\boldsymbol{C}_{6\times6} = \begin{bmatrix} \backslash 1 \backslash & \backslash 0 \backslash & \backslash 0 \backslash \\ \backslash -\frac{3}{2} \backslash & \backslash 2 \backslash & \backslash -\frac{1}{2} \backslash \\ \backslash \frac{1}{2} \backslash & \backslash -1 \backslash & \backslash \frac{1}{2} \backslash \end{bmatrix},$$

$$\boldsymbol{A}_{6\times6} = \begin{bmatrix} \backslash \frac{1}{2} \backslash & \backslash \frac{2}{3} \backslash & \backslash 1 \backslash \\ \backslash \frac{2}{3} \backslash & \backslash \frac{\pi}{4} \backslash & \backslash \frac{16}{15} \backslash \\ \backslash 1 \backslash & \backslash \frac{16}{15} \backslash & \backslash \frac{4}{3} \backslash \end{bmatrix}$$

where $\backslash * \backslash = \begin{bmatrix} * & 0 \\ 0 & * \end{bmatrix}$.

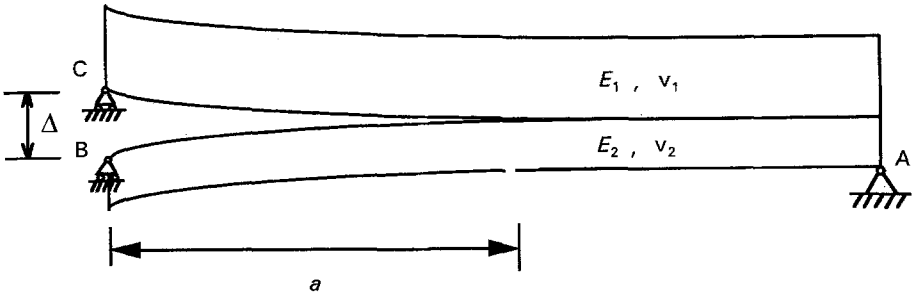

Figure A2 Boundary condition for BEM calculation. The vertical and horizontal displacement at point A are fixed to be 0. The vertical displacement at point B is given as 0. The vertical displacement at point C is given as Δ.

For each specimen, the crack closure method gives one G value. This G value was compared with the G values from Equation A5 using the displacements corresponding to different pairs of nodal points behind the crack tip (Fig. A1). The G values obtained from both methods are very close to each other. In the ADCB specimen case, the G values using the opening displacement from nodes b and b' agree best with that obtained using the virtual crack closure method. So in our calculations, the value of Δu_x and Δu_y from points b and b' are used to compute the phase angle, ψ_d, using Equations A1 and A3.

The accuracy of our BEM program is checked by comparing its results with those of known closed-form solutions. Our BEM results agree well (to within 3%) with these solutions. We also compared our BEM results with the finite element method results of an interface crack problem solved by Charalambides *et. al.* [16]. For typical cases, our results differ by no more than 5%. Details of the numerical calculation are given elsewhere [27].

References

1. R. FAYT, R. JÉRÔME and PH. TEYSSIÉ, *J. Polym. Sci. Polym. Phys. Ed.* **27** (1989) 775.
2. R. FAYT and PH. TEYSSIÉ, *Polym. Eng. Sci.* **29** (1989) 538.
3. C. CRETON, E. J. KRAMER and G. HADZIIOANNOU, *Macromolecules* **24** (1991) 1846.
4. H. R. BROWN, *ibid.* **22** (1989) 2859.
5. C. CRETON, E. J. KRAMER, C. Y. HUI and H. R. BROWN, *ibid.* **25** (1992) 3075 (see also C. CRETON, PhD Thesis, Cornell University, Ithaca, NY 1992).
6. J. W. SMITH, E. J. KRAMER, F. XIAO, C. Y. HUI, W. REICHERT and H. R. BROWN, *J. Mater. Sci.*, in press.
7. J. R. RICE, *J. Appl. Mech.* **55** (1988) 98.
8. Z. SUO and J. W. HUTCHINSON, *Mater. Sci. Eng.* **A107** (1990) 135.
9. *Idem, Int. J. Fract.* **43** (1990) 1.
10. C. F. SHIH, *Mater. Sci. Eng.* **A143** (1991) 77.
11. F. ERDOGAN and G. C. SIH, *J. Basic Eng. Trans. ASME* **85** (1963) 519.
12. C. H. WU, *J. Elasticity* **8** (1978) 235.
13. H. C. CAO, B. J. DAGLEISH and A. G. EVANS, *Closed Loop* **23** (1990) 3929.
14. A. G. EVANS, B. J. DAGLEISH, M. HE and J. W. HUTCHINSON, *Acta. Metall.* **37** (1989) 3249.
15. M. RUHLE, A. G. EVANS, M. F. ASHBY and J. P. HIRTH (eds), "Metal-Ceramic Interfaces, Acta-Scripta Metallurgica Proceedings," Series 4 (Pergamon Press, New York, 1990).
16. P. G. CHARALAMBIDES, J. LUND, A. G. EVANS and R. M. McMEEKING, *J. Appl. Mech.* **56** (1989) 77.
17. N. P. O'DOWD, M. G. STOUT and C. F. SHIH, *Philos. Mag. A.* **66** (1992) 1037.
18. K. M. LIECHTI and Y. S. CHAI, *J. Appl. Mech.* **59** (1992) 295.
19. H. R. BROWN, *J. Mater. Sci.* **25** (1990) 2791.
20. J. WASHIYAMA, C, CRETON and E. J. KRAMER, *Macromolecules*, **25** (1992) 4751.
21. L. C. FELDMAN and J. W. MAYER, "Fundamentals of Surface and Thin Film Analysis" (North-Holland, New York, 1986).
22. J. WASHIYAMA, E. J. KRAMER and C. Y. HUI, *Macromolecules* submitted.
23. F. XIAO C. Y. HUI, J. WASHIYAMA and E. J. KRAMER, in preparation.
24. M. F. KANNINEN, *Int. J. Fract.* **9** (1973) 83.
25. D. S. DUGDALE, *J. Mech. Phys. Solids* **8** (1960) 100.
26. L. L. BERGER, *Macromolecules* **22** (1989) 3162.
27. F. XIAO, C. Y. HUI and E. J. KRAMER, in preparation.

Received 9 February
and accepted 24 February 1993